Boundary Layer Loss Mechanism and Justification of Wall Functions for Turbulence Modeling

Ge-Cheng Zha*
Dept. of Mechanical Engineering
University of Miami
Coral Gables, Florida 33124
E-mail: zha@apollo.eng.miami.edu

Abstract

The mechanism of entropy creation in an adiabatic boundary layer is studied. The local entropy creation rate has two sources: shear stress work and heat flux gradient. These two factors have the same order of magnitude everywhere in the boundary layer. Their balance results in a fairly uniform distribution of entropy creation rate across the boundary layer. In the inner layer region, the large rate of entropy creation due to the velocity gradient and shear stress is offset by the gradient of the heat flux. The heat flux gradient is so large that a negative entropy creation region is generated in the inner layer. With the new theory of the entropy creation mechanism, the wall function methods for the internal turbulent flow loss prediction are justified. Detailed theoretical derivation and numerical proof are given in the paper. The previous theory of local entropy creation mechanism in a boundary layer given by Denton ignored the important heat flux gradient factor. Denton's theory will lead to a large false error when it is used to study the applicability of wall function methods to loss prediction. The numerical solutions of a transonic cascade using wall functions and integrating to the wall are compared. The difference for the loss prediction using these two methods is small and is consistent with the error range given from the loss mechanism theory of this paper.

1 Introduction

As Denton pointed out in his well known article "Loss Mechanisms in Turbomachines" [1], the measure of performance for internal flows is the loss, which is directly related to the efficiency of a machine. This is different from the external flows, where the surface forces (e.g. skin friction, lift) are usually of the interest. Denton gave the in depth analysis of the loss mechanisms for various sources including boundary layer, mixing, shock waves, heat transfer, end wall, tip clearance, etc. Denton emphasized that the use of correlations to predict the loss should not be a substitute for trying to understand the origin of the loss, and suggested that a good physical understanding of the latter may be more valuable than a quantitative prediction.

The loss of an internal flow is determined by the entropy creation. Hence entropy is usually used to study the loss mechanism. For the boundary layer loss mechanism, Denton derived the total rate of entropy creation across an adiabatic boundary layer as the following:

$$\dot{S}_a = \frac{d}{dx}\int_0^\delta (\rho V_x(s - s_\delta))dy = \int_0^\delta \frac{1}{T}\tau_{xy}dV_x \quad (1)$$

This means that the shear stress work is the sole source for the entropy creation of an adiabatic boundary layer. Eq.(1) represents the integral of the local entropy creation rate multiplied by the mass flow rate. If eq.(1) is divided by the total mass across the boundary layer, it is the usually defined mass averaged total rate of entropy creation across the boundary layer. If eq.(1) is normalized by $\rho_e u_e^3/T$, it is called dissipation coefficient. Denton further extended the conclusion of eq.(1) to the local rate of entropy creation within a boundary layer as:

$$\dot{S}_v = \frac{1}{T}\tau\frac{dV}{dy} \quad (2)$$

Following this thought, Denton presented the plots of τ_{xy} vs V_x for several typical turbulent boundary layers with and without pressure gradient, which indicate that most of the entropy cre-

* Associate Professor

ation is within the viscous sublayer and the logarithm region. Denton also referred Dawes's results [2], which shows that 90% of the entropy generation occurs within the inner part of a turbulent boundary layer.

The inner layer is a very thin layer from the solid wall surface to logarithm layer (2% to 20% of the boundary layer thickness[3]) compared with the overall thickness of a turbulent boundary layer. Denton's conclusions mean that the thick outer layer actually has very little entropy creation. Denton hence further indicated that the entropy creation may be insensitive to the detailed state of a boundary layer since usually only the outer layer is greatly affected by the streamwise pressure gradient.

If all of the above conclusions are true, we then face a serious challenge: the widely used wall function boundary conditions are wrong to predict the flow loss. The concept of wall functions is to make use of the law of the wall to avoid resolving the inner layer of a turbulent boundary layer when the transport equations of the turbulence are solved, for example, $k-\epsilon$ model, $k-\omega$ model, Reynolds Stress Equation model[4][5], etc. The advantage of using wall functions is that it is more CPU efficient. The first grid point is usually located in the logarithm layer, i.e., $30 \leq y^+ \leq 150$. However, inferring from Denton's theory[1], we may conclude that wall function methods, which ignore the inner layer where most of the entropy is created, will significantly under-predict the loss and can not be used for internal flows[6].

Wall functions can calculate the surface skin friction fairly accurately as long as the boundary layer is not separated. Wall functions were therefore first used for external flows. When it was used for internal flows, few questions were asked why the wall function methods can predict the flow loss by neglecting the high gradient sublayer. As indicated by eq.(1), the loss of an internal flow is determined by the integral across the boundary layer, not only the forces on the surface. Even though no study has been done to justify using wall functions for loss prediction, wall functions have been popularly used for internal flows. For example, the famous APNASA code developed by Adamczyk [7] for multi-stage turbomachines uses wall functions for its $k-\epsilon$ turbulence model. For the popularly used commercial CFD solver, Fluent, version 6 (the latest version), the standard option for $k-\epsilon$ model uses wall functions (see Fluent User's Guide). For the past two decades of CFD development and application, it seems that people haven't complain too much about the dramatic error caused by wall functions for loss prediction. The conventional wisdom may have some merit.

Strictly speaking, wall functions only exist when the turbulent boundary layer is attached. However, people use wall functions for all kinds of flows, separated or attached. The argument is, when the flow is separated, other models do not necessarily predict the flow better. Wall function concept is not only used for RANS (Reynolds averaged Navier-Stokes equations) methods, it is sometimes also employed for LES(Large Eddy Simulation). This paper is not to advocate using wall function methods, but to clarify some theoretical misconception.

Now, the question is: can the wall functions really be used for internal turbulent flow loss prediction (assume the boundary layer is attached)? The first objective of this paper is to answer this question. To do so, we have to re-visit the issue of loss mechanism of a turbulent boundary layer, because it seems conflicting between the Denton's loss mechanism theory[1] and using wall functions. Hence the second objective of this paper is to re-examine the loss mechanism for a boundary layer. Following Denton's article[1], we primarily focus on the adiabatic boundary layers.

The study of this paper found that the local rate of entropy creation given in Denton's theory, eq.(2), is incorrect, even though the total rate of the entropy creation of eq.(1) is correct. The local rate of eq.(2) has ignored a very important contribution to entropy creation caused by the heat flux gradient. This contribution is canceled out for the total rate of entropy creation when integrated across the boundary layer. It is shown that, when the heat flux gradient is considered, the actual error of entropy creation rate caused by using wall functions is small and acceptable.

With the advent of high speed computers, numerical solutions of complicated flow problems are commonly used. Under this circumstance, understanding of the fundamental physical mechanism becomes more important to interpret the numerical techniques and solutions. The effort of this paper is to fill some gap between the numerics and physics.

According to the findings of the loss mechanism is this paper, the following speculation may be inferred: For incompressible flow computation, if the energy equation is not solved and the wall functions are used, the loss prediction may have a large discrepancy because the entropy creation due to the heat flux gradient is not available. This topic is beyond the scope of this paper and needs to be studied separately.

2 The Concept of Wall Functions

A turbulent boundary layer may be considered as being composed of three layers: the viscous sublayer, the logarithm layer, and the defect layer. The viscous sublayer and the logarithm layer is also called inner layer and the defect layer is called outer layer. The inner layer is not as sensitive as the outer layer to the flow history and free stream variation.

The logarithm layer is close enough to the wall surface that the convection can be neglected yet distant enough that the viscous stress is negligible, because it is in the fully turbulent region. The distance from the wall to the logarithm layer is usually about 10% of the whole boundary layer thickness. The law of the wall holds in the logarithm layer. For incompressible flow, the law of the wall may be expressed as[3]:

$$u^+ = \frac{1}{k} ln y^+ + B \tag{3}$$

where k is the Kármán constant, k=4.1, B=5.0,

$$u^+ = u/u_\tau, \qquad y^+ = u_\tau y/\nu, \qquad u_\tau = \sqrt{\tau_w/\rho}$$

where u is the velocity, y the distance from the wall, τ_w the friction shear stress on the wall.

The viscous sublayer is between the wall surface and the logarithm layer and the viscous shear stress is dominant in that region. From the wall surface to the logarithm layer, the total shear stress composed of viscous and turbulent shear stress is nearly constant.

Based on the above characteristics of the logarithm layer, asymptotic solution can be obtained for some high Reynolds number turbulent kinetic energy and dissipation transport equations. The $k-\epsilon$ and $k-\omega$ models have the following wall functions[4]:

$$k = \frac{u_\tau^2}{\sqrt{\beta^*}}, \qquad \omega = \frac{k^{1/2}}{\beta^{*1/4} k y}, \qquad \epsilon = \beta^{*3/4} \frac{k^{3/2}}{ky} \tag{4}$$

where β^* is a constant.

Employing the above wall functions in the logarithm layer with the range of y^+ typically from 30 to 150, a CFD solver with $k-\epsilon$ and $k-\omega$ turbulence model can avoid resolving the viscous sublayer and a part of the logarithm layer. Fig.1 shows a sketch of a CFD grid using wall functions. The first grid line above the wall is located within the logarithm layer of the turbulent boundary layer. The CFD solution covers the domain above the first grid line and there is no solution between the wall and the computational domain. However, with the correlation of the law of the wall, eq.(3), and the wall functions, eq.(4), the surface friction shear stress τ_w can be calculated fairly accurately as long as the boundary layer is not separated.

Since using wall functions does not need to resolve the viscous sublayer, where there exists a large velocity gradient and a very fine mesh is required, the computation is much more CPU efficient than those resolving the viscous sublayer. This is the main reason that the wall function methods are widely used.

According to eq.(1), the total rate of entropy creation

$$\dot{S}_a = \int_0^\delta \frac{1}{T} \tau_{xy} dV_x = \int_0^{y_{wallfunction}} \frac{1}{T} \tau_{xy} dV_x + \int_{y_{wallfunction}}^\delta \frac{1}{T} \tau_{xy} dV_x \tag{5}$$

As mentioned before, $y_{wallfunction}$ is located in the logarithm layer with y^+ usually in the range of $30 \le y^+ \le 150$. Since there is no CFD solution between wall and $y_{wallfunction}$. The first term of the integral in eq.(5) is ignored. The total rate of the entropy creation becomes:

$$\dot{S}_a = \int_{y_{wallfunction}}^\delta \frac{1}{T} \tau_{xy} dV_x \tag{6}$$

According to Denton's theory[1], the ignored term from eq.(5) to eq.(6) generates most of the entropy creation since the velocity increases most rapidly from the viscous sublayer to the logarithm layer, and the shear stress is about constant in that region. Indeed, Zha[8] found that, when the $y_{wallfunction}$ varies from $y^+ = 30$ to 150, 60% to 90% of the total rate of entropy creation is missed according to eq.(6). Such a large discrepancy should be reflected by the total pressure loss, which is related to the entropy creation by the following relation:

$$\Delta S = -R ln \frac{Pt_2}{Pt_1} \tag{7}$$

However, the numerical investigation did not show such a dramatic error for the total pressure loss when wall functions are used[8]. The puzzle

has been the motivation leading to the present paper.

3 Boundary Layer Loss Mechanism

To study the boundary layer loss mechanism, we will begin with the steady state boundary layer equations[3] for a flat plate.

Continuity equation:

$$\frac{\partial(\rho u)}{\partial x} + \frac{\partial(\rho v)}{\partial y} = 0 \tag{8}$$

X-momentum equation:

$$\rho(u\frac{\partial u}{\partial x} + v\frac{\partial u}{\partial y}) = -\frac{\partial p}{\partial x} + \frac{\partial \tau_{xy}}{\partial y} \tag{9}$$

Y-momentum equation:

$$\frac{\partial p}{\partial y} \approx 0 \tag{10}$$

Energy equation:

$$\rho(u\frac{\partial h}{\partial x} + v\frac{\partial h}{\partial y}) = u\frac{\partial p}{\partial x} - \frac{\partial q}{\partial y} + \tau_{xy}\frac{\partial u}{\partial y} \tag{11}$$

where u, v are the velocity component in x- and y- direction, p the pressure, ρ the density, h the static enthalpy, q the heat flux, τ_{xy} the shear stress. q and τ_{xy} may be determined as:

$$q = -(k_m + k_t)\frac{dT}{dy} \tag{12}$$

$$\tau_{xy} = (\mu_m + \mu_t)\frac{du}{dy} \tag{13}$$

where k_m and μ_m are the molecular thermal conductivity and molecular viscosity, k_t and μ_t are the turbulent thermal conductivity and turbulent viscosity.

Use the substantial derivative:

$$\frac{D}{Dt} = \frac{\partial}{\partial t} + u\frac{\partial}{\partial x} + v\frac{\partial}{\partial y} \tag{14}$$

and steady state flow condition,

$$\frac{\partial}{\partial t} = 0$$

the energy equation combined with the y-momentum eq. can be written as

$$\rho\frac{Dh}{Dt} = \frac{Dp}{Dt} - \frac{\partial q}{\partial y} + \tau_{xy}\frac{\partial u}{\partial y} \tag{15}$$

From the thermodynamic relation:

$$dh = Tds + \frac{1}{\rho}dp \tag{16}$$

the energy equation can be further written as:

$$T\frac{Ds}{Dt} = \frac{1}{\rho}(\tau_{xy}\frac{\partial u}{\partial y} - \frac{\partial q}{\partial y}) \tag{17}$$

or

$$T(u\frac{\partial s}{\partial x} + v\frac{\partial s}{\partial y}) = \frac{1}{\rho}(\tau_{xy}\frac{\partial u}{\partial y} - \frac{\partial q}{\partial y}) \tag{18}$$

Multiply dy on both sides of eq.(18) and rearrange the terms, we have

$$\frac{\partial s}{\partial x}(\rho u dy) + \frac{\partial s}{\partial y}(\rho v dy) = \frac{1}{T}(\tau_{xy}\frac{\partial u}{\partial y}dy - \frac{\partial q}{\partial y}dy) \tag{19}$$

$\rho u dy$ is actually the mass flow rate going through a streamtube with the hight of dy, hence if let

$$d\dot{m} = \rho u dy \tag{20}$$

Eq.(19) becomes

$$(\frac{\partial s}{\partial x} + \frac{v}{u}\frac{\partial s}{\partial y})d\dot{m} = \frac{1}{T}(\tau_{xy}\frac{\partial u}{\partial y}dy - \frac{\partial q}{\partial y}dy) \tag{21}$$

v/u is the slope of the streamline. If assume θ is the angle between the streamline and x axis, then

$$\frac{v}{u} = \frac{sin(\theta)}{cos(\theta)} \tag{22}$$

Eq.(21) then becomes

$$(cos(\theta)\frac{\partial s}{\partial x} + sin(\theta)\frac{\partial s}{\partial y})d\dot{m} = \frac{cos(\theta)}{T}(\tau_{xy}\frac{\partial u}{\partial y}dy - \frac{\partial q}{\partial y}dy) \tag{23}$$

The content inside the parenthesis on the left hand side of eq.(23) is the derivative of the entropy along the streamline. Let l be the length along a streamline, then eq.(23) can be written as:

$$\frac{\partial s}{\partial l}d\dot{m} = \frac{cos(\theta)}{T}(\tau_{xy}\frac{\partial u}{\partial y}dy - \frac{\partial q}{\partial y}dy) \tag{24}$$

For a boundary layer along a flat plate, the streamline angle is nearly zero, that is $cos(\theta) \approx 1$.

Hence, the energy equation of a boundary layer along a flat plate may be expressed as:

$$\frac{\partial s}{\partial l}d\dot{m} = \frac{1}{T}(\tau_{xy}\frac{\partial u}{\partial y} - \frac{\partial q}{\partial y})dy \tag{25}$$

The right hand side of eq.(25) may be simplified by using

$$\frac{\partial u}{\partial y}dy \approx du, \qquad \frac{\partial q}{\partial y}dy \approx dq \tag{26}$$

Then we have

$$\frac{\partial s}{\partial l}d\dot{m} = \frac{1}{T}(\tau_{xy}du - dq) \qquad (27)$$

The assumptions of eq.(26) are reasonable for flat plate boundary layer even though they are not mathematically rigorous.

Eq.(27), which is equivalent to eq.(25), says that the local entropy creation rate along a streamtube within a boundary layer is caused by the shear stress work and heat flux variation. As long as there is temperature gradient, dq and dq/dy are not zero. $\tau_{xy}du$ and dq have the same order of magnitude. That is why they are kept in the boundary layer equations after the dimensionless analysis[3].

The total rate of the entropy creation, $\dot{S}_a$, can be obtained by integrating eq.(25) or (27). That is:

$$\dot{S}_a = \int_0^{\dot{m}_\delta} \frac{\partial s}{\partial l}d\dot{m} = \int_0^{\delta} \frac{1}{T}(\tau_{xy}\frac{\partial u}{\partial y} - \frac{\partial q}{\partial y})dy \qquad (28)$$

or

$$\dot{S}_a = \int_0^{\dot{m}_\delta} \frac{\partial s}{\partial l}d\dot{m} = \int_0^{\delta} \frac{1}{T}(\tau_{xy}du - dq) \qquad (29)$$

where $\dot{m}_\delta$ stands for the total mass flow across the boundary layer.

When wall functions are used, above formulations become:

$$\dot{S}_a = \int_{\dot{m}_{wallfunction}}^{\dot{m}_\delta} \frac{\partial s}{\partial l}d\dot{m}$$

$$= \int_{y_{wallfunction}}^{\delta} \frac{1}{T}(\tau_{xy}\frac{\partial u}{\partial y} - \frac{\partial q}{\partial y})dy \qquad (30)$$

or

$$\dot{S}_a = \int_{\dot{m}_{wallfunction}}^{\dot{m}_\delta} \frac{\partial s}{\partial l}d\dot{m}$$

$$= \int_{y_{wallfunction}}^{\delta} \frac{1}{T}(\tau_{xy}du - dq) \qquad (31)$$

For an adiabatic boundary layer, on the wall surface and at the edge of the boundary layer, $q = 0$. Hence from eq.(29), we have

$$\int_0^{\dot{m}_\delta} \frac{\partial s}{\partial l}d\dot{m} = \int_0^{\delta} \frac{1}{T}\tau_{xy}du \qquad (32)$$

This means that the total rate of entropy creation across a boundary layer is equal to the total shear stress work in the boundary layer, which is the same as Denton's conclusion, eq.(1). However, simply extend eq.(32) to determine the local rate of entropy creation as eq.(2) is incorrect. The local rate of entropy creation is determined by eq.(25) or (27). The dq in eq.(27), or $\frac{\partial q}{\partial y}dy$ in eq.(25), has a very important contribution to the local entropy creation. It is just canceled out after doing the integral across the boundary layer.

In other words, when we say that the total rate of entropy creation across a boundary layer is equal to the shear stress work, it is only correct in the quantitative sense. It is misled if think it actually occurs that way. Physically, both heat flux variation and shear stress work cause entropy creation. These two factors always co-exist and interact each other everywhere in the whole boundary layer.

If we now explain the applicability of wall functions using eq.(28) and (25) instead of eq.(1) and (2), it is found that the accuracy of using wall functions to predict the internal flow loss is acceptable. This will be shown in the following sections.

Even though eq.(29) and (28) may be considered as equivalent, we prefer to use eq.(28) to analyze the entropy creation in the following sections. There are two reasons for this: 1) eq.(28) is mathematically more rigorous than eq.(29); 2) the terms in eq.(28) are well defined and are easier to calculate numerically.

It needs to point out that the present derivation follows the similar strategy of Denton[1]. The major difference is that, when we consider the local rate of entropy creation, we start from eq.(25), Denton started from eq.(32), which has no heat flux variation.

4 Entropy Creation in a Boundary Layer

An ideal gas turbulent boundary layer in an adiabatic flat duct is solved numerically using Fluent CFD solver to obtain the database for analysis. The duct flow has no pressure gradient. A freestream Mach number of 0.2 is selected so that the flow is in the incompressible regime, which will facilitate the validation of the numerical solutions. The duct flow with freestream Mach number of 0.95 is then computed to examine if the compressible and incompressible boundary layers behave similarly for entropy creation. The conclusion is they behave the same. To save the space, only the results of the incompressible turbulent boundary

layer is presented.

4.1 Solution Validation

The duct has an aspect ratio of 25. The Reynolds number based on the duct height is $Re_h = 10^5$. Fig.2 shows the velocity vector field near the duct exit. The no slip adiabatic boundary conditions are imposed on the solid wall. The mesh size is 101x81. The two equation $k-\epsilon$ model is used with the low Reynolds number model integrating to the wall. The y^+ for the first grid adjacent to the wall is, $y_1^+ = 1.8$. Even though we want to study the entropy creation predicted by using the wall functions, the benchmark solution needs to be integrated to the wall so that the whole boundary layer profile can be obtained. The solutions with wall function boundary conditions are a subset of the solution integrated to the wall. Hence the evaluation of using the wall functions will be still based on the results from the solution integrated to the wall.

A duct cross section close to the duct outlet is chosen for analyzing the turbulent boundary layer profiles. The Reynolds number based on the momentum thickness at that location is $Re_\theta = 3584.5$, the shape factor $H = 1.34$. The velocity profile of the inner layer is compared with the law of the wall using the formulation of Spalding[3]. Fig.3 shows that the computed velocity profile agrees very well with the law of the wall.

The dissipation coefficient, Cd, is integrated according to the following definition:

$$Cd = \frac{T\dot{S}_d}{\rho_e u_e^3} \tag{33}$$

where

$$\dot{S}_d = \int_0^\delta \frac{1}{T}\tau_{xy}\frac{du}{dy}dy \tag{34}$$

There is little difference if $\dot{S}_d$ is integrated as in eq.(1), that is

$$\dot{S}_d = \int_0^\delta \frac{1}{T}\tau_{xy}du \tag{35}$$

The computed value of Cd is, $Cd = 0.001463$, which agrees very well with the value of 0.001432 calculated by using the correlation given in [9]:

$$Cd = 0.0056Re_\theta^{-1/6} \tag{36}$$

As aforementioned, the variation of the heat flux is crucial to determine the local rate of entropy creation. Therefore, the accuracy of the temperature profile is very important. Fig.4 shows that the computed temperature profile agrees excellently with that given by Crocco-Busemann formulation[3], which is

$$T = T_w + (T_{aw} - T_w)\frac{u}{u_e} - \frac{0.88u^2}{2Cp} \tag{37}$$

This formulation was obtained with the assumption of $Pr = Pr_t \approx 1$, which is close to the ideal gas used in the current case. For the adiabatic boundary layer in the present case, the wall temperature is equal to the adiabatic wall temperature. Hence the second term in eq.(37) is canceled. The boundary layer ends at about $y^+ = 1650$. Therefore fig.4 is the temperature profile for the whole boundary layer.

Above results indicate that the present numerical solution resolves the turbulent boundary layer fairly accurately, which is sufficient to provide the database for further entropy creation analysis.

4.2 Entropy Creation Analysis

First, let us see fig.5, which is the distribution of the local entropy creation due to the shear stress work. According to Denton's definition given in eq.(2), this is the local rate of entropy creation. The total area under the curve is the total rate of entropy creation across the boundary layer as defined in eq.(1), or eq.(32). Similar plot is also presented in[1]. As pointed out by Denton[1], most of the entropy creation occurs in the inner layer. For the present case at $y^+ = 30$, it takes about 62% of the total area. For $y^+ = 107$, it is 78% of the area. Obviously, inferred from Denton's theory, the wall functions located in the logarithm layer with $30 \le y^+ \le 150$ will miss most of the entropy creation, or the loss prediction.

Now, let us see the contribution of the local entropy creation from the two terms of eq.(25) and their resultant as shown in Fig.6. The dash line is $\tau_{xy}du/dy$ vs y, which is the same curve as fig.5, but in a slightly different variable form. We drop 1/T here for simplicity since T is relative constant compared with the variation of $\tau_{xy}du/dy$ and dq/dy. Fig.7 shows the zoomed part of fig.6 near the wall. $\tau_{xy}du/dy$ has very large value near the wall due to the large velocity gradient. This again shows that the near wall region takes most of the area under the dash line as indicated in fig.5.

However, the heat flux gradient near the wall is also very large and is in the same order of magnitude as the shear stress work. The large rate of en-

tropy creation due to $\tau_{xy}du/dy$ is offset by the heat flux gradient. On the wall surface, the $\tau_{xy}du/dy$ is greater than the dq/dy and results in the maximum entropy creation rate on the wall surface(see fig.7). Above the viscous sublayer, the dq/dy increases more rapidly than the $\tau_{xy}du/dy$ and creates a local negative valley of the rate of entropy creation very close to the wall with the y^+ from about 5 to 20 (the solid line). This means that the inner layer is not the region that most of the entropy is created.

The solid line in fig.6 shows that the resultant local rate of entropy creation (eq.(25)) is fairly uniform for most part of the boundary layer except near the wall and gradually reduce to zero at the edge of the boundary layer. Through the whole boundary layer, the $\tau_{xy}du/dy$ and dq/dy have the same order of magnitude. The integral of the total rate of entropy creation is the area under the solid line according to eq.(28). This area is equal to area of fig.5 quantitatively. It is also equal to the area under the dash line in the same plot of fig.6. However, it can be seen that the area distribution of the solid line is much more uniform than fig.5 and the dash line across the boundary layer in fig.6.

For the integral of the total rate of entropy creation, the negative area of the local rate of entropy creation (solid line) will cancel a part of the positive area (see fig.7). In other words, there exists one point on the right side of the negative valley, from which the integrated area will be equal to the total area integrated from the wall surface under the solid line. Let this point be termed as balance point. The estimated location of the balance point is between y^+ =25 to 30 according to the numerical results. This means if the wall function location starts from the balance point, the total rate of entropy creation is quantitatively the same as integrating from the wall. The offset of the $\tau_{xy}du/dy$ and dq/dy near the wall dramatically reduce the dependence of the total rate of entropy on the near wall region. This means that, if wall function boundary conditions are used in the inner layer, the total rate of entropy creation estimated by eq.(30) will have much less error than that estimated solely from the shear stress work as in eq.(6). The correct quantitative loss prediction can be obtained if the wall function location is at the balance point.

To understand the behavior of dq/dy, we can see the heat flux distribution across the adiabatic boundary layer as shown in fig.8. The heat flux is determined according to eq.(12). On the wall surface, the heat flux $q = 0$. The heat flux then rapidly increase with very large gradient and reaches the peak at about $y^+ = 250$. Such a large gradient is attributed to two factors: 1)the large temperature gradient near the wall as shown in fig.4; 2) the large increase of the turbulent thermal conductivity near the wall. The positive heat flux gradient near the wall has the effect to offset the entropy creation rate due to the large velocity gradient as shown in fig.7. After the peak (see fig.8), the heat flux gradually reduce to zero at the edge of the boundary layer with negative gradient, which has the positive contribution to the rate of entropy creation. As shown in fig.6, for the outer layer of the boundary layer layer, the negative heat flux gradient is the dominant contributor to the entropy creation. Through out the whole boundary layer, the shear stress work and heat flux gradient compensate for each other and make the distribution of the local entropy creation fairly uniform. In summary, in the inner layer, the heat flux q has positive gradient that reduces the local entropy creation rate. In the outer layer, the heat flux has the negative gradient that increases the local entropy creation rate.

As explained for eq.(32), because $q = 0$ on the wall surface and at the edge of the boundary layer, the integral of the heat flux gradient across the whole boundary layer is zero. That is the area under the dash-dot-dot line in fig.6 is zero. In other words, the integral of the heat flux gradient across the boundary layer does not have a net contribution to the total rate of entropy creation. Again, this is only correct in the quantitative sense. The heat flux gradient makes the local entropy creation more uniform through out the boundary layer. If the integral of the total rate of entropy creation does not start from the wall surface as in eq.(30) when wall functions are used, the integral of the heat flux will not be zero because $q \neq 0$ at $y_{wallfunction}$. In fact, it has a dominant contribution to the total rate of entropy creation.

4.3 Entropy Creation Rate with Wall Functions

With the above analysis, we can examine the effect of using wall functions on the total rate of entropy creation rate. To clearly see the contribution of each term, the integral of shear stress work and heat flux gradient of eq.(30) are separated as the following:

$$\dot{S}_a = \int_{\dot{m}_{wallfunction}}^{\dot{m}_\delta} \frac{\partial s}{\partial l} d\dot{m}$$

$$= \int_{y_{wallfunction}}^{\delta} \frac{1}{T}\tau_{xy}\frac{\partial u}{\partial y}dy - \int_{y_{wallfunction}}^{\delta} \frac{\partial q}{\partial y}dy \quad (38)$$

Eq.(38) can be normalized by $\rho_e u_e^3/T_e$. That is:

$$\dot{S}_a = Cd - Ch \quad (39)$$

where

$$Cd = \frac{T_e}{\rho_e u_e^3}\int_{y_{wallfunction}}^{\delta} \frac{1}{T}\tau_{xy}\frac{\partial u}{\partial y}dy \quad (40)$$

$$Ch = \frac{T_e}{\rho_e u_e^3}\int_{y_{wallfunction}}^{\delta} \frac{\partial q}{\partial y}dy \quad (41)$$

Obviously, Cd, Ch and $\dot{S}_a$ will vary with the location of the $y_{wallfunction}$. Fig.9 shows such variations. The dash-dot-dot line is the total rate of entropy creation integrated from the wall surface as defined in eq.(28).

When integrated from the wall surface, as explained for eq.(32), the following results are expected:

$$\dot{S}_a \approx Cd, \quad Ch \approx 0 \quad (42)$$

The following are the values obtained

$Cd = 0.00146343$, $Ch = -0.00000553$, $\dot{S}_a = Cd - Ch = 0.00146896$.

The dash-dot-dot line in fig.9 has the value of $\dot{S}_a$, which is used as the benchmark solution for comparison.

$y_{wallfunction}$ needs to be located in the logarithm layer and is usually in the range of y^+ =30 - 150. Fig.9 shows that when $y^+_{wallfunction}$ varies from 30 to 170, Cd alone is significantly lower than the benchmark total rate of the entropy creation. When the contribution of Ch is added, the computed total rate of entropy creation using wall functions, the solid line, is very close to the benchmark solution. In particular, if the $y^+_{wallfunction}$ has the low value such as 30, the difference of the computed total rate of entropy creation from the benchmark solution is negligible. The contribution due to Ch is about twice larger than the shear stress work, Cd, at $y^+_{wallfunction} = 30$ and five times larger at $y^+_{wallfunction} = 150$.

Fig.10 shows the quantitative error of the computed total rate of entropy creation at different $y_{wallfunction}$. If only the shear stress work is considered as the total rate of entropy creation given in eq.(6), the error is from 62% to 82% when the $y^+_{wallfunction}$ varies from 30 to 170. When the heat flux gradient is added, the error is dramatically reduced to 0.34% to 7.8%. For loss prediction in engineering application, this error range is within the prediction uncertainty and is acceptable. In particular, if the wall functions are used at y^+ about 30, the difference of the loss prediction between using wall functions and integrating to the wall is negligible. The reason that the error is so small at $y^+ =$ 30 is because it is close to the balance point located between $y^+ = 25-30$. As aforementioned, the total rate of entropy creation is quantitatively correct if the wall functions are located on the balance point.

We may draw two conclusions form these results:

1) the local rate of entropy creation should include two terms, the shear stress work and heat flux gradient for the adiabatic boundary layer. The definition with shear stress work only given by Denton in eq.(2) neglects a very important contribution from the heat flux gradient.

2) with the new understanding of the entropy creation mechanism in an adiabatic boundary layer, the wall function method is proved to be acceptable to predict internal flow loss under the condition that the boundary layer is not separated.

The following speculation may be inferred from above conclusions: For incompressible flow computation, sometimes the energy equation is not solved when the temperature filed is not of the interest. In this case, if wall functions are used, the loss prediction may have a large discrepancy because the entropy creation due to the heat flux gradient is not available. This topic is beyond the scope of this paper and needs to be studied separately.

A case of compressible flow with Mach number of 0.95 for the duct shows the same behavior as the incompressible case, both qualitatively and quantitatively. To save space, the results of the Mach 0.95 case is not shown here.

5 Comparing Cascade Solutions Using Wall Functions and Integrating to Wall

A simple transonic cascade flow is calculated to compare the loss prediction using wall functions and integrating to the wall. The purpose is to ex-

amine if the error range of the loss prediction falls within the theoretical range given in the previous analysis.

The example is a 2D cascade with NACA0012 airfoil. The solidity is 1.0, inlet Mach number is 0.51, Reynolds number based on chord is 0.97×10^6, incidence angle is zero.

The Fluent software and the $k-\epsilon$ model are again used to provide the CFD solutions. Two solutions are obtained. The first solution is the the benchmark solution resolving the boundary layer to the wall surface. The second solution uses wall function boundary conditions to treat the wall. The solutions are then compared for their loss prediction.

The code is validated for the same 2D duct flow in previous section by using wall functions. The velocity profile agrees very well with the law of the wall starting from the logarithm region. The temperature profile also agrees well with the Crocco-Busemann formulation. To save space, the validation results for the 2D duct boundary layer using wall functions are not presented here.

Fig.11 shows the grid of the cascade for the solution using wall functions. The hybrid grid is used. The body fitted hexahedral O-mesh is used around the airfoil to resolve the boundary layer. Outside of the boundary layer mesh is the tetrahedral mesh to reduce the number of the mesh cells. The mesh generation is designed to try to make the two grids have the same grid density in the same region, if possible. The same O-mesh area is used for both the meshes. Along the airfoil surface there are totally 230 mesh points for both solutions. The number of the mesh points on the periodic boundaries, inlet and outlet are the same for the two solutions. This will make the number of mesh cells the same for both solutions outside of the O-mesh area.

The only difference for the meshes of the two solutions are the number of grid points normal to the blade surface inside the O-mesh domain. For the solution integrating to the wall, the y_1^+ from the leading edge to trailing edge varies from 1.6 to 0.2. For the solution with wall function, the y_1^+ varies from 160 to 50. Therefore, the first solution needs to have more grid points than the second solution in the direction normal to the wall. There are totally 60 grid points in the direction normal to the wall for the first solution. Among them, 25 are between the wall surface and the wall function location of the second solution. There are 35 points between the wall function location and the O-mesh boundary. For the second solution using wall functions, between the wall function location and the O-mesh boundary, the maximum number of grid points that can fit in the space is 30 when the minimum stretching factor f=1.0 is used. That means that there are 5 points less than the solution integrating to the wall between the wall function location and O-mesh boundary. Since in the outer layer the boundary layer gradient is much less than the inner layer, 30 points is sufficient to resolve the outer layer and little difference is expected between using 30 and 35 points.

Fig.12 is the Mach number contours of the two solutions, the top one is the solution using wall functions, and the bottom one is the solution integrating to the wall. It shows that there is a normal shock in the aft airfoil region. The Mach number before the shock is 1.24 and the shock is not strong enough to cause a flow separation. Hence this is a good case to compare the loss prediction of the wall function methods. There is no distinguishable difference for the Mach contours of these two solutions.

Fig.13 is the static pressure distributions for the two solutions. Again, they agree excellently. The static pressure distributions indicate that the flow is accelerated to supersonic, and then is decelerated by the normal shock to subsonic, then further diffused to the cascade exit. Fig.14 is the total pressure distributions in the wake region $\frac{1}{4}$ chord downstream of the trailing edge. The wake width and depth agree very well for these two solutions. The wake of the wall function solution is slightly deeper than the one integrating to the wall. The total pressure loss is 3.66% for the solution integrating to the wall , and 3.63% for the solution using wall functions. The difference is 0.8%, which is small and is in the error range of the previous analysis.

To see the details of the flow field difference integrating to the wall and using wall functions, fig.15 shows the zoomed mesh in the region of the trailing edge for the solution integrating to the wall. The mesh is very dense near the wall to resolve the inner layer. The first mesh has the $y^+ = 0.2$. Fig.16 is the velocity vector in the trailing edge region. Even though the trailing edge radius is small, there are still two counter rotating vortices generated due to the low base pressure above and below the symmetric line.

Fig.17 is the mesh imposed with the velocity vector field in the region of the trailing edge for the solution using wall functions. The first mesh has the $y^+ = 50$. Obviously, the grid spacing is much larger than the first solution and there is no mesh to resolve the viscous sublayer. No detailed

trailing edge vortices are resolved. However, neglecting these details does not really reduce the accuracy of the loss prediction as shown in the wake profile (fig.14) and the small difference of the loss prediction value, 0.8%. According to the new understanding of the loss mechanism in the boundary layer, it is explainable that such a good loss prediction using wall functions is due to the entropy creation balanced by the shear stress work and the heat flux gradient in the boundary layer.

6 Conclusions

The mechanism of entropy creation in an adiabatic boundary layer is studied. The local entropy creation rate has two sources: shear stress work and heat flux gradient. These two factors have the same order of magnitude everywhere in the boundary layer. Their balance results in a fairly uniform distribution of entropy creation rate across the boundary layer. In the inner layer region, the large rate of entropy creation due to the velocity gradient and shear stress is offset by the gradient of the heat flux. The heat flux gradient is so large that a negative entropy creation region is generated in the inner layer. Theoretically, there exists a balance point in the inner layer. If the wall functions are located at the balance point, the loss prediction using wall functions and integrating to the wall will be the same. With the new theory of the entropy creation mechanism, the study justifies that the wall function methods are applicable to internal flow loss prediction. For a Mach 0.2 adiabatic boundary layer in a 2D duct with no pressure gradient and no separation, the error of the total rate of entropy creation varies from 0.34% to 7.8% when the wall functions are applied at $y^+ = 30 - 170$. This error is within the engineering application uncertainty. The compressible flow case of Mach 0.95 shows the same behavier as the incompressible case.

The previous theory of entropy creation mechanism in a boundary layer given by Denton does not include the heat flux gradient factor. The sole contribution to the local entropy creation rate is the shear stress work. Using Denton's theory to study the applicability of wall function methods for internal flow loss prediction will lead to a very large unacceptable error in the range of 60% to 80%. According to the new theory developed in this paper, such a large error is false and is due to ignoring the heat flux gradient contribution to the local rate of entropy creation.

The numerical solutions of a transonic cascade using wall functions and integrating to the wall are compared. The wake profiles of these two solutions agree very well. The difference of the loss prediction using these two methods is small and is consistent with the error range given from the loss mechanism theory of this paper.

From the new loss mechanism theory, the following speculation may be inferred, but not proved: For incompressible flow computation, if the energy equation is not solved and the wall functions are used, the loss prediction may have a large discrepancy because the entropy creation due to the heat flux gradient is not available. This topic is beyond the scope of this paper and is not studied herein.

7 Acknowledgment

This paper is originated from the author's course project at MIT[8]. The author would like to thank Prof. E. Greitzer at MIT for his encouragement to pursue this work. The GRSA from the University of Miami to support this research is acknowledged.

References

[1] J. Denton, "Loss Mechanisms in Turbomachines," *Journal of Turbomachinery*, vol. 115, pp. 621–656, 1993.

[2] W. Dawes, "A Comparison of Zero and One Equation Turbulence Modeling for Turbomachinery Calculations." ASME Paper 90-GT-303, June 1990.

[3] F. M. White, *Viscous Fluid Flow, 2nd edition.* McGraw-Hill, Inc, 1991.

[4] D. Wilcox, *Turbulence Modelling for CFD.* DCW Industries, Inc., 1993.

[5] G.-C. Zha and D. D. Knight, " Computation of 3D Shock/Turbulent Boundary Layer Interaction Using a Reynolds Stress Equation Turbulence Model ," *AIAA Journal*, vol. 34, pp. 1313–1320, 1996.

[6] G.-C. Zha, K. Dalbey, and B. Van Poppel, " Flow Network Optimization for TOBI Nozzle to Turbine Blade Pre-Swirl coolant System ." Course Project Report No. 3, MIT, March 5, 2000.

[7] J. J. Adamczyk, "Aerodynamic Analysis of Multistage Turbomachinery Flows in Support of Aerodynamic Design," *Journal of Turbomachinery*, vol. 122, pp. 189–217, 2000.

[8] G.-C. Zha, "The Defect of Computing Losses Using Wall Functions for Turbulent Internal Flows." Project Report No. 2, Course 16.51, Internal Flows, MIT,, March 28, 2000.

[9] Hermann Schlichting, *Boundary Layer Theory.* McGraw-Hill Book Company, Inc, 1966.

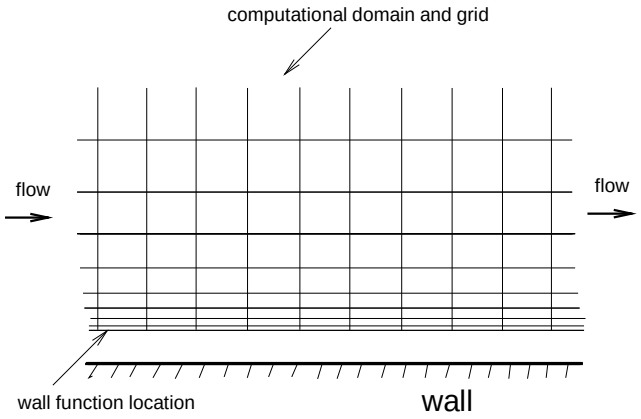

Figure 1: A sketch of the wall function location and computational domain

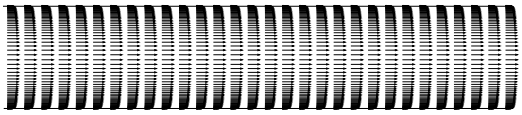

Figure 2: Velocity vector field of the turbulent boundary layer in the duct near exit, $M_{freestream} = 0.2$

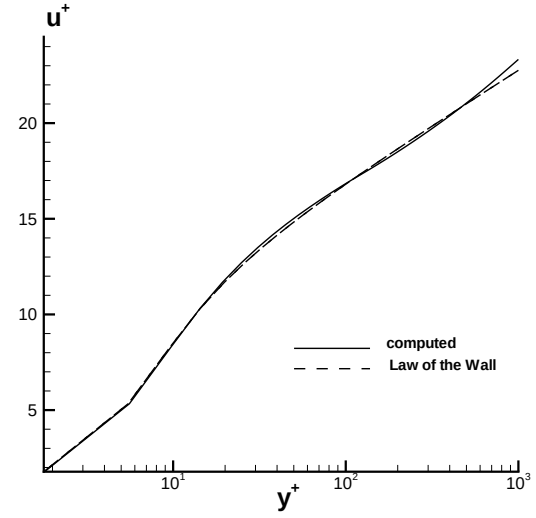

Figure 3: Computed velocity profile in the inner layer compared with the law of the wall.

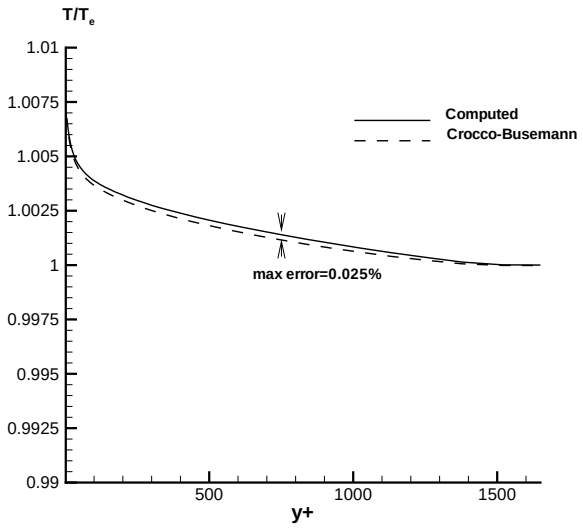

Figure 4: Computed temperature profile of the turbulent boundary layer compared with Crocco-Busemann solution.

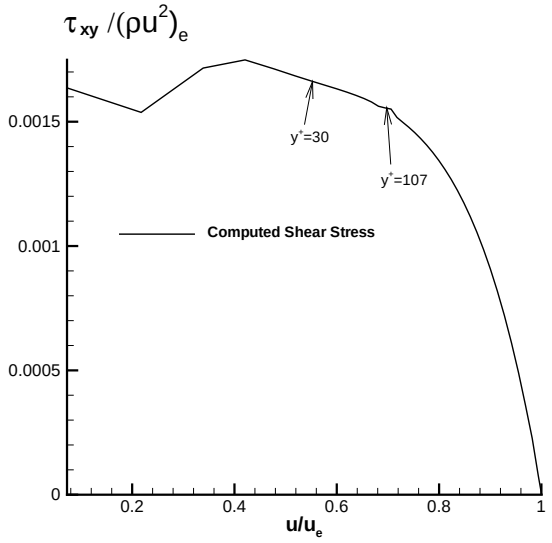

Figure 5: The distribution of entropy creation due to shear stress work across the boundary layer.

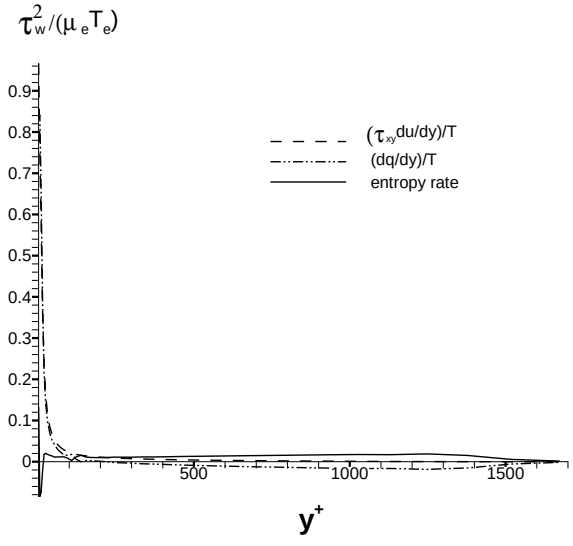

Figure 6: The distribution of entropy creation across the boundary layer for individual terms and their resultant.

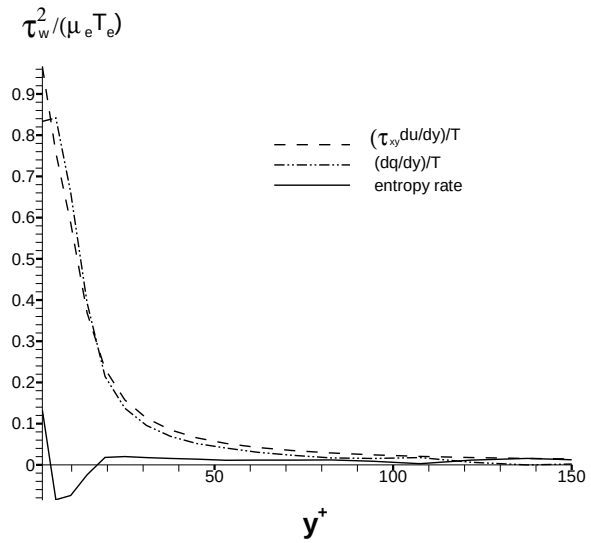

Figure 7: The distribution of entropy creation near the wall for individual terms and their resultant.

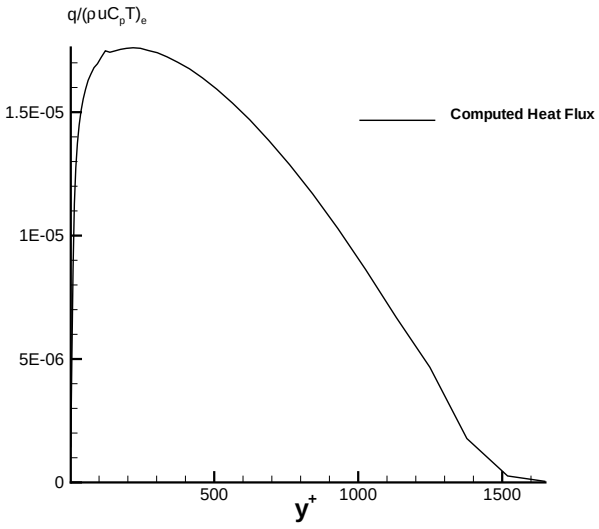

Figure 8: Heat flux distribution for the duct adiabatic boundary layer.

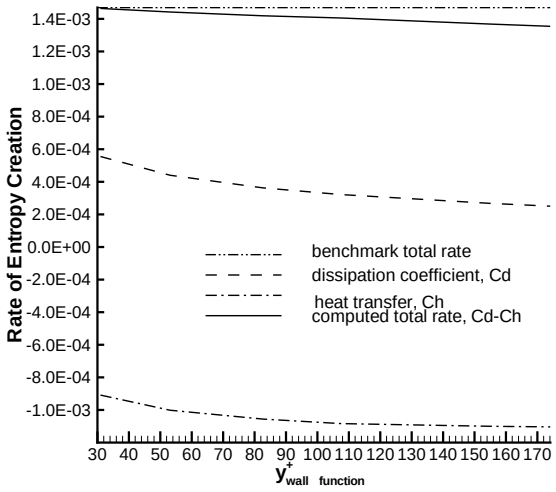

Figure 9: Entropy creation rate computed at different wall function location.

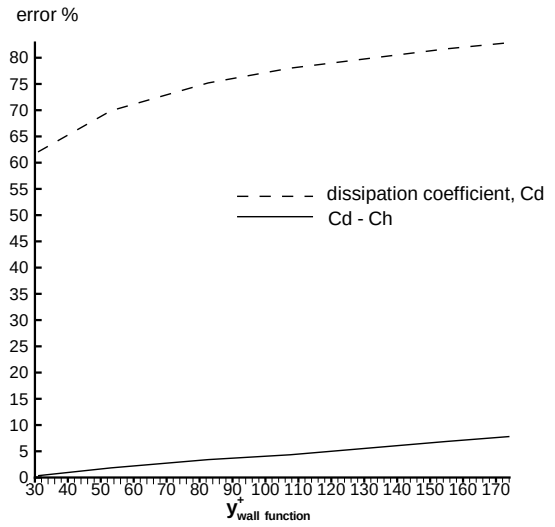

Figure 10: Error of the total entropy creation rate computed at different wall function location.

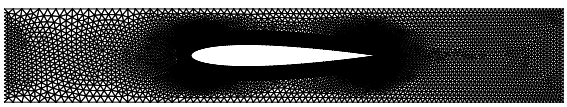

Figure 11: Mesh for the NACA0012 cascade solution integrating to the wall.

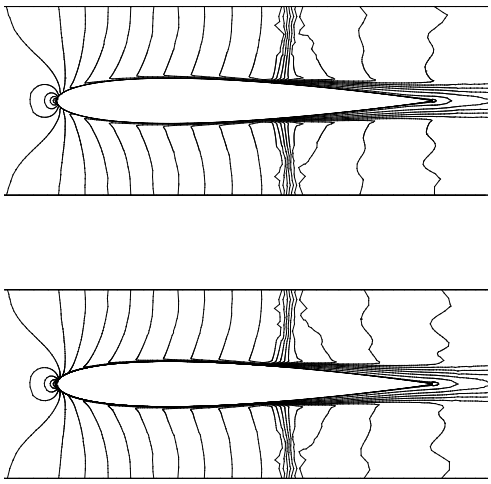

Figure 12: Mach number contours of the cascade, top: using wall functions; bottom: integrating to the wall.

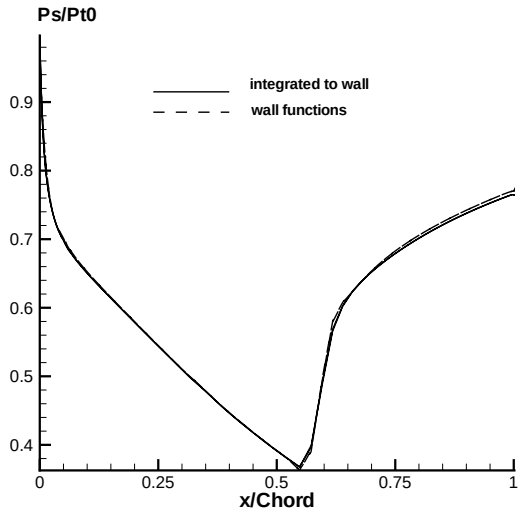

Figure 13: Static pressure distributions of the cascade flow solutions using wall functions and integrating to the wall.

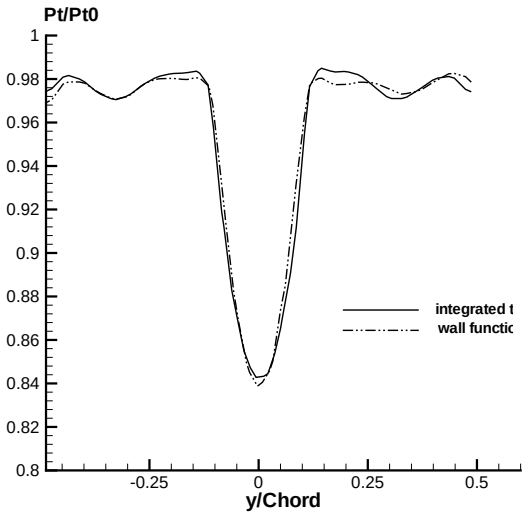

Figure 14: Total pressure distributions in the wake region for the cascade flow solutions using wall functions and integrating to the wall.

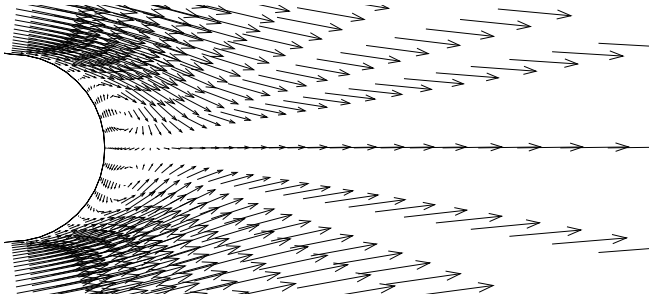

Figure 16: Velocity vector field in the trailing edge region for the solution integrating to the wall.

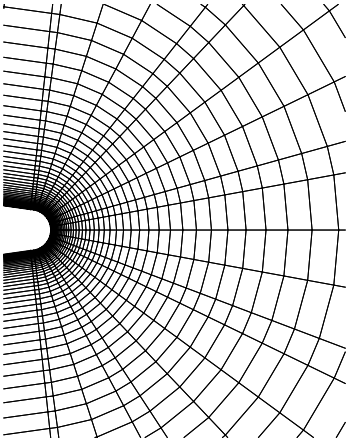

Figure 15: Mesh in the trailing edge region for the solution integrating to the wall.

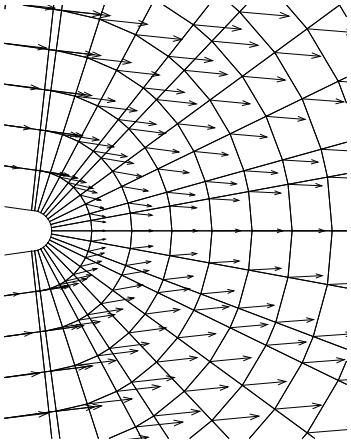

Figure 17: Mesh and velocity vector field in the trailing edge region for the solution using wall functions.